High-resolution spectroscopy of the $2^2\Pi_u \leftarrow X^4\Sigma_g^-$ forbidden transitions of C_2^+

Christopher G. Tarsitano, Christopher F. Neese, and Takeshi Oka[a)]
Department of Chemistry, University of Chicago, Chicago, Illinois 60637; Department of Astronomy and Astrophysics, University of Chicago, Chicago, Illinois 60637; and The Enrico Fermi Institute, University of Chicago, Chicago, Illinois 60637

(Received 25 May 2004; accepted 9 July 2004)

The electronic absorption spectrum of the (0,2), (1,3), and (6,9) bands of the $B^4\Sigma_u^- - X^4\Sigma_g^-$ system of C_2^+ was obtained using the velocity modulation technique in conjunction with heterodyne detection. The rotationally resolved spectrum shows perturbations, which are attributed to the $2^2\Pi_u$ state. The mixing between the $B^4\Sigma_u^-$ state and the $2^2\Pi_u$ state for nearly degenerate levels generated enough intensity borrowing to observe twenty $2^2\Pi_u \leftarrow X^4\Sigma_g^-$ forbidden transitions. The parameters of a model Hamiltonian were fit to the bands and their corresponding forbidden transitions. Line position measurements, line strength factors, and expectation values for the orbital angular momentum $\langle \Lambda' \rangle$ for the forbidden transitions are reported. Molecular parameters from the global fit of each band, including their corresponding forbidden transitions, are reported. © *2004 American Institute of Physics.* [DOI: 10.1063/1.1787493]

I. INTRODUCTION

The molecular ion C_2^+ is conjectured to be an important species in the extraterrestrial medium. Using a satellite-born mass spectrometer, C_2^+ has been detected in the comet Halley[1] and proposed to be present in the comet Giacobini-Zinner.[2] This ion is predicted to play a role in the chemistry of the interstellar medium.[3–5]

In 1972, Meinel obtained a rotationally resolved spectrum at 249 nm and assigned it to a $^2\Sigma_g^- - ^2\Pi_u$ transition of C_2^+.[6] While the spectroscopic evidence suggests that the species is C_2^+, several theoretical treatments disagree with this assignment.[7,8] Later, O'Keefe and co-workers obtained a low resolution spectrum of C_2^+ using translational energy spectroscopy.[9] Using the calculations of Petrongolo *et al.*,[7] they were able to assign several electronic transitions.

This work was followed by the definitive work of Maier and co-workers who obtained the matrix spectrum of C_2^+ and later obtained many bands of the $B-X$ system in the gas phase.[10–13] In their high-resolution gas-phase work, Maier and co-workers observed perturbations in the quartet splitting of the spectrum. While their experiment had the resolution to do a rotational analysis, the resolution was not sufficient for a detailed analysis of the spin-spin interaction or the perturbation. However, Maier and co-workers did predict that the perturbation was the result of a spin–orbit interaction with the $2^2\Pi_u$ state, so named by Petrongolo *et al.*[7] since the richness of electronic states of C_2^+ defies the use of ordinary alphabetic nomenclature. Maier's prediction was based on the calculations of Petrongolo *et al.*, which showed that the $2^2\Pi_u$ state lies ≈0.5 eV below the minimum of the $B^4\Sigma_u^-$ state.[7,12] This prediction was validated in two spectroscopic analyses that followed by Zackrisson and Royen[14] and Boudjarane, Carré, and Larzillière[15] who analyzed the effect of the perturbation on the levels of the perturbed $B^4\Sigma_u^-$ state.

In this paper, we present the direct observations of the $2^2\Pi_u \leftarrow X^4\Sigma_g^-$ forbidden transitions of C_2^+. From a rotational analysis of the perturbations in the (0,2), (1,3), and (6,9) bands of the $B-X$ system of C_2^+, we were able to predict forbidden transitions from the $X^4\Sigma_g^-$ state to the $2^2\Pi_u$ state and their relative intensities. Twenty forbidden lines were measured and included in a least-squares fit of each band. In addition to the observed forbidden lines, we predict others whose intensities lied just below our detection limit or were overlapped with other lines. The expectation value of the orbital angular momentum $\langle \Lambda' \rangle$ was experimentally determined and presented to characterize the amount of Π character in the perturbing levels.

II. EXPERIMENT

The experimental setup is shown schematically in Fig. 1. We employed a double-modulation technique, velocity modulation with heterodyne detection, to improve the sensitivity of the spectrometer. The first technique, velocity modulation, developed by Gudeman, Saykally *et al.*, provides the ion/neutral discrimination needed in the analysis of the spectrum.[16,17] The second technique, heterodyne detection, developed by Bjorklund, permits the laser radiation to be modulated at radio/microwave frequencies and thus further improves the sensitivity of the spectrometer.[18] The double-modulation technique reduces the problem of residual amplitude modulation, which degrades the sensitivity enhancement of heterodyne detection alone. In this technique the spectral lines associated with ions have a line shape resembling a second-derivative Gaussian, whereas the transitions from neutral species have a line shape resembling a first-

a)Electronic mail: t-oka@uchicago.edu

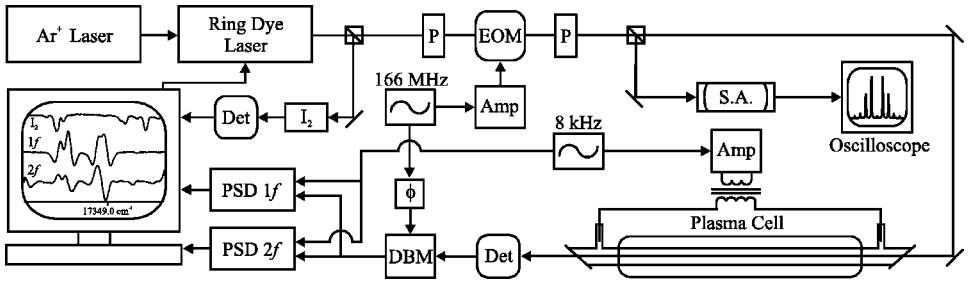

FIG. 1. A schematic diagram of the absorption spectrometer using velocity modulation with heterodyne detection. The radiation from an Ar^+-pumped dye laser passes through a polarizer (P), an electro-optic phase modulator (EOM), and another polarizer before traversing the plasma cell and impinging upon a fast photoreceiver (Det). The signal from the detector is demodulated by a double balanced mixer (DBM), whose local oscillator source is the signal generator driving the EOM passed through a phase shifter (ϕ). A pair of phase sensitive detectors (PSDs) then demodulates this signal at $1f$ and $2f$, where f is the discharge frequency of the plasma. Demodulation produces the characteristic second-derivative line shape for ions at $1f$ and first-derivative line shape for ions and neutrals at $2f$. Shown on the computer screen is the R(9) quartet of the (1,3) band from the $B-X$ system of C_2^+. Beamsplitters before and after the EOM send diagnostic beams through an I_2 cell and spectrum analyzer, respectively. The spectrum analyzer is used to monitor the depth of the modulation which is observed on an oscilloscope. The absorption from the I_2 cell is recorded along with the experimental spectrum and is compared against the wavelength meter to ensure proper wavelength meter behavior.

derivative Gaussian. A variant of this technique was developed by Wang *et al.*, who also use the magnetic rotation effect.[19]

The radiation source consisted of a Coherent 899-29 Autoscan ring laser that was pumped by a Coherent Innova 200 Ar^+ laser. The dye, Rhodamine 6G, provided an output power of more than several hundred milliwatts in the region of 17 085–17 450 cm^{-1} with a linewidth of 500 kHz. Data collection and control of the laser was accomplished via Coherent autoscan software. The absolute uncertainty in the frequency determined by the wavelength meter of the Coherent ring laser was 0.007 cm^{-1}. An iodine spectrum was recorded to ensure proper wavelength meter behavior.[20,21]

The laser output was passed through a polarizer and a $MgO:LiNbO_3$ electro-optical phase modulator (EOM) driven at 166 MHz. An etalon was used to monitor the depth of the modulation. By monitoring the signal strength of a C_2^+ transition and adjusting the rf voltage across the $MgO:LiNbO_3$ crystal, the optimal modulation index was experimentally determined to be ≈ 2.3 or a carrier-to-sideband ratio, $0\text{th}:1\text{st}:2\text{nd}:3\text{rd}:4\text{th} \approx 0.05:1.0:0.58:0.13:0.02$. Then, the sidebanded beam was passed through the discharge cell and the absorption signal was detected using a New Focus fast photoreceiver. The ac signal from the detector was first mixed down using a double balance mixer and then demodulated at $1f$ and $2f$ using a pair of Stanford Research System SR510 lock-in amplifiers. The use of $1f$ and $2f$ detection helps further discriminate the signals of ionic and neutral molecules.

The laser was step-scanned in 25 MHz increments. For each step, 500 data points per channel were acquired and averaged. The time constant of the lock-in amplifiers and the scanning rate of the laser were optimized by repeatedly scanning over a C_2^+ transition and monitoring the spectral line so that there were no distortions to the line shape or shifts in the rest frequency. It was determined that the optimal settings for the scanning rate and time constant were 167 MHz/s and 300 ms, respectively. For the weaker transitions, an average of 15 000 data points per step were used with a scan rate and time constant of 17 MHz/s and 3 s, respectively.

The C_2^+ molecular ions were produced in a water-cooled positive column discharge. In brief, the reagent gases (5.1 Torr He and 10 mTorr of CO) flowed into a discharge cell through 18 inlets and pumped out by a mechanical pump through 9 outlets. The bore of the discharge had a length of 1.3 m and an inner diameter of 12 mm. The plasma was produced by applying a potential of several kilovolts at 8 kHz across the electrodes. The resulting discharge current was ≈ 125 mA rms. Carbon monoxide was used as a reagent gas in preference to C_2H_2 because C_2H_2 produced C_2^- efficiently and the bands of the $B-X$ system of C_2^- interfered with the spectrum of C_2^+. However, the (1,2) band of the $A-X$ system of CO^+ was detected within the (1,3) band of C_2^+, and C_2H_2 was used to differentiate the species.

III. THEORY

A. Effective Hamiltonian and matrix elements

An effective Hamiltonian is derived from the fundamental molecular Hamiltonian via an electronic contact transformation followed by a vibrational contact transformation. We use the derivation of Brown *et al.*[22] except that we allow the $2\,^2\Pi_u$ and $B^4\Sigma_u^-$ states to remain coupled through the electronic contact transformation. Thus, in addition to the effective Hamiltonians describing the $2\,^2\Pi_u$ and $B^4\Sigma_u^-$ states, there is an effective Hamiltonian describing the interaction of the two states. The derivation of the effective Hamiltonian for the unperturbed $X^4\Sigma_g^-$ state follows the derivation of Brown *et al.* exactly.

The Hamiltonians for the $^4\Sigma$ states, H_Σ, and the $^2\Pi$ state, H_Π, are given in Eqs. (1) and (2), respectively,

$$H_\Sigma = T_\Sigma + B_\Sigma \mathbf{N}^2 - D_\Sigma \mathbf{N}^4 + \gamma_\Sigma \mathbf{N}\cdot\mathbf{S} + \gamma_{\Sigma D}\mathbf{N}^2\mathbf{N}\cdot\mathbf{S} + \frac{2}{3}\lambda_\Sigma(3S_z^2 - \mathbf{S}^2), \quad (1)$$

$$H_\Pi = T_\Pi + B_\Pi \mathbf{N}^2 - D_\Pi \mathbf{N}^4 + A_\Pi L_z S_z + \tfrac{1}{2} A_{\Pi D}(L_z S_z \mathbf{N}^2 + \mathbf{N}^2 L_z S_z) + \tfrac{1}{2} p_\Pi (\Lambda_+^2 S_- N_- + \Lambda_-^2 S_+ N_+) - \tfrac{1}{2} q_\Pi (\Lambda_+^2 N_-^2 + \Lambda_-^2 N_+^2). \quad (2)$$

The above Hamiltonians are written in terms of $\mathbf{N}=\mathbf{J}-\mathbf{S}$ instead of $\mathbf{R}=\mathbf{J}-\mathbf{S}-\mathbf{L}$. While $\mathbf{R}$ appears in the fundamental molecular Hamiltonian, $\mathbf{N}$ does not contain terms coupling different electronic states and is more appropriate for the effective Hamiltonians. The ladder operators $\Lambda_\pm^2$ are defined by Brown *et al.*[22] The interaction Hamiltonian H' for the coupling between the $2^2\Pi_u$ and $B^4\Sigma_u^-$ states is not readily written in operator notation, but the matrix elements of H' are derived in Sec. III B.

Table I lists the matrix elements of the effective Hamiltonians. Several papers give these matrix elements in differing detail.[14,15,23] All matrix elements are evaluated using a Wang-transformed Hund's case *a* basis,

$$|n^{2S+1}\Lambda_\Omega v J_e^f\rangle = \frac{1}{\sqrt{2}}|v\rangle(|n\Lambda\rangle|S\Sigma\rangle|J\Omega\rangle \mp (-1)^s|n\ -\Lambda\rangle|S\ -\Sigma\rangle|J\ -\Omega\rangle). \quad (3)$$

In Eq. (3), n is an index specifying the particular electronic state, f_e is the rotationless parity,[24] and $s=1$ for Σ^- states and $s=0$ for all other states. The off-diagonal matrix elements are evaluated using the phase conventions defined by

$$\langle S\Sigma|\sigma_{xz}|S-\Sigma\rangle = (-1)^{S-\Sigma}, \quad (4a)$$

$$\langle \Lambda|\sigma_{xz}|-\Lambda\rangle = (-1)^{-\Lambda}, \quad (4b)$$

where σ_{xz} is the symmetry operator corresponding to reflection in the *xz* plane of the molecule.

B. Effective interaction Hamiltonian

The term in the fundamental molecular Hamiltonian responsible for coupling the $2^2\Pi_u$ and $B^4\Sigma_u^-$ states is the spin–orbit term, H_{SO}. The matrix elements of the interaction Hamiltonian H', prior to the vibrational contact transformation, are given to the second order by

$$\langle 2^2\Pi_{u\Omega};r|H'|B^4\Sigma_{u\Omega}^-;r\rangle = \langle 2^2\Pi_{u\Omega};r|H_{SO}|B^4\Sigma_{u\Omega}^-;r\rangle + \sum_n \frac{[\frac{1}{2}V_\Sigma(r)+\frac{1}{2}V_\Pi(r)-V_n(r)]\langle 2^2\Pi_{u\Omega};r|H_{SO}|n;r\rangle\langle n;r|H_{SO}|B^4\Sigma_{u\Omega}^-;r\rangle}{[V_\Sigma(r)-V_n(r)][V_\Pi(r)-V_n(r)]}. \quad (5)$$

TABLE I. Matrix elements for the $^2\Pi$ and $^4\Sigma^-$ states of a diatomic molecule ($x=J+1/2$).

$\langle n^4\Sigma_{3/2}^- v J_e^f|H|n^4\Sigma_{3/2}^- v J_e^f\rangle = T_\Sigma + 2\lambda_\Sigma + B_\Sigma(x^2-1) - D_\Sigma(x^4+x^2-2) - \frac{3}{2}\gamma_\Sigma - 3\gamma_{\Sigma D}(x^2-1)$

$\langle n^4\Sigma_{1/2}^- v J_e^f|H|n^4\Sigma_{1/2}^- v J_e^f\rangle = T_\Sigma - 2\lambda_\Sigma + B_\Sigma(x^2\pm 2x+3) - D_\Sigma[(x^4+13x^2+6)\pm(4x^3+12x)] - \gamma_\Sigma(\pm x+\frac{7}{2}) - \gamma_{\Sigma D}[7x^2+9\pm(x^3+10x)]$

$\langle n^4\Sigma_{3/2}^- v J_e^f|H|n^4\Sigma_{1/2}^- v J_e^f\rangle = -\left[B_\Sigma - 2D_\Sigma(x^2\pm x+1) - \frac{\gamma_\Sigma}{2} - \frac{\gamma_{\Sigma D}}{2}(x^2\pm 2x+6)\right]\sqrt{3x^2-3}$

$\langle n^2\Pi_{3/2} v J_e^f|H|n^2\Pi_{3/2} v J_e^f\rangle = T_\Pi + \frac{A_\Pi}{2} + \left(B_\Pi + \frac{A_{\Pi D}}{2}\right)(x^2-1) - D_\Pi(x^4-x^2)$

$\langle n^2\Pi_{1/2} v J_e^f|H|n^2\Pi_{1/2} v J_e^f\rangle = T_\Pi - \frac{A_\Pi}{2} + \left(B_\Pi - \frac{A_{\Pi D}}{2}\right)(x^2+1) - D_\Pi(x^4+3x^2) \mp \left(\frac{p_\Pi}{2}+q_\Pi\right)x$

$\langle n^2\Pi_{3/2} v J_e^f|H|n^2\Pi_{1/2} v J_e^f\rangle = -\left[B_\Pi - 2D_\Pi x^2 \mp \frac{q_\Pi}{2}x\right]\sqrt{x^2-1}$

$\langle n'^4\Sigma_{3/2}^- v' J_e^f|H|n^2\Pi_{3/2} v J_e^f\rangle = -\frac{1}{2}\xi_{3/2} - \frac{1}{2}\xi_D(x^2-1)$

$\langle n'^4\Sigma_{1/2}^- v' J_e^f|H|n^2\Pi_{1/2} v J_e^f\rangle = -\frac{1}{2\sqrt{3}}\xi_{1/2} - \frac{1}{2\sqrt{3}}\xi_D(x^2\pm x+2)$

$\langle n'^4\Sigma_{3/2}^- v' J_e^f|H|n^2\Pi_{1/2} v J_e^f\rangle = \frac{1}{2}\xi_D\sqrt{x^2-1}$

$\langle n'^4\Sigma_{1/2}^- v' J_e^f|H|n^2\Pi_{3/2} v J_e^f\rangle = \frac{1}{\sqrt{3}}\xi_D\sqrt{x^2-1}$

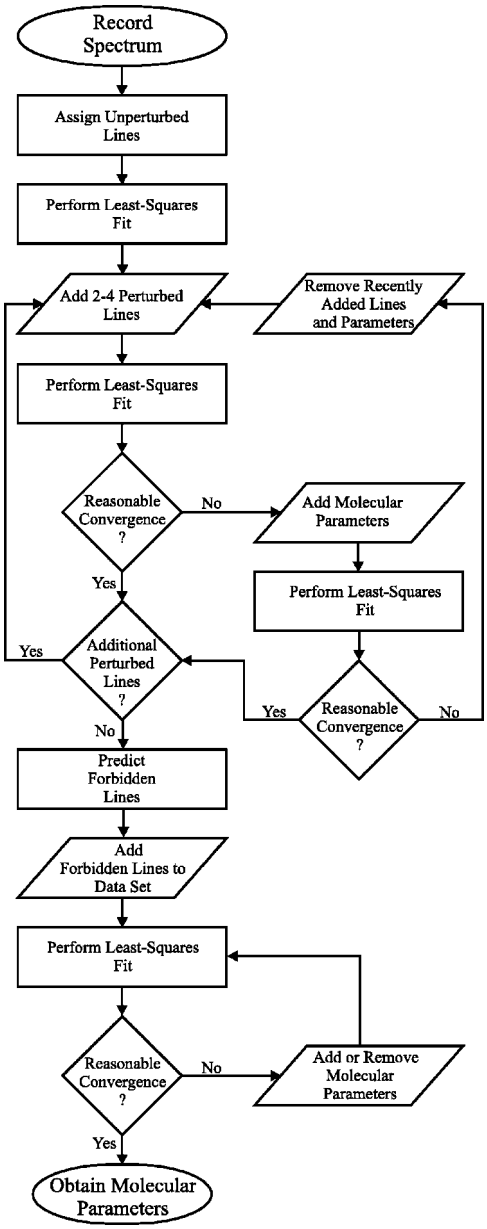

FIG. 2. A flowchart describing the analysis of a band in the spectrum. An iterative approach was used to fit the perturbations in the bands. From this fit, the line positions and relative intensities of forbidden transitions were predicted. The forbidden transitions were included in a final least-squares fit of each band and molecular parameters were obtained.

In Eq. (5), n indexes all electronic states except for the $2^2\Pi_u$ and $B^4\Sigma_u^-$ states.[30] The $|B^4\Sigma_{u\Omega}^-;r\rangle$, $|2^2\Pi_{u\Omega};r\rangle$, and $|n;r\rangle$ are electronic state vectors solving the electronic Schrödinger equation as a function of the internuclear distance r, and the $V_\Sigma(r)$, $V_\Pi(r)$, $V_n(r)$ are the corresponding eigenvalues, i.e.,

$$H_{elec}|B^4\Sigma_{u\Omega}^-;r\rangle = V_\Sigma(r)|B^4\Sigma_{u\Omega}^-;r\rangle, \tag{6a}$$

$$H_{elec}|2^2\Pi_{u\Omega};r\rangle = V_\Pi(r)|2^2\Pi_{u\Omega};r\rangle, \tag{6b}$$

$$H_{elec}|n;r\rangle = V_n(r)|n;r\rangle. \tag{6c}$$

The Wigner-Eckart theorem leads to a general expression for the spin–orbit matrix elements appearing in Eq. (5).[25,26]

$$\langle S',\Sigma',\Lambda',\Omega|H_{SO}|S,\Sigma,\Lambda,\Omega\rangle = (-1)^{S'-\Sigma'}\begin{pmatrix} S' & 1 & S \\ \Sigma' & -\Delta\Sigma & -\Sigma \end{pmatrix}\langle S',\Lambda'\|H_{SO}\|S,\Lambda\rangle, \tag{7}$$

where $\Delta\Omega=0$ and $\Delta\Lambda=-\Delta\Sigma$. There is an additional symmetry to the reduced matrix elements given by Eq. (7), due to parity,

$$\langle S',\Lambda'=-1\|H_{SO}\|S,\Lambda=0^\pm\rangle = \pm\langle S',\Lambda'=1\|H_{SO}\|S,\Lambda=0^\pm\rangle. \tag{8}$$

This symmetry is needed to Wang transform the basis set.

Using Eqs. (5)–(8), the interaction between the $B^4\Sigma_u^-$ and $2^2\Pi_u$ states after the electronic contact transformation is

$$\langle 2^2\Pi_{u3/2};r|H'|B^4\Sigma_{u3/2}^-;r\rangle = \frac{-\xi_{3/2}(r)}{2}, \tag{9a}$$

$$\langle 2^2\Pi_{u1/2};r|H'|B^4\Sigma_{u1/2}^-;r\rangle = \frac{-\xi_{1/2}(r)}{2\sqrt{3}}. \tag{9b}$$

Equations (9a) and (9b) define the molecular parameters $\xi_{3/2}(r)$ and $\xi_{1/2}(r)$. It is evident from Eq. (5) that $\xi_{3/2}(r)$ and $\xi_{1/2}(r)$ are each the sum of a first-order and second-order contribution. The first-order contribution is the reduced matrix element, $\langle S',\Lambda'\|H_{SO}\|S,\Lambda\rangle$, from Eq. (7) and is the same for both $\xi_{3/2}(r)$ and $\xi_{1/2}(r)$. We expect the first-order contribution to be more significant than the second-order contribution; therefore, $\xi_{3/2}(r)\approx\xi_{1/2}(r)$.

The vibrational contact transformation of the terms defined above is straightforward. After the second-order vibrational contact transformation, there are three molecular constants describing the perturbation, $\xi_{3/2}$, $\xi_{1/2}$, and ξ_D. The centrifugal distortion terms are easily derived by taking the anticommutator of the matrix defined by Eqs. (9a) and (9b) and the matrix of the $\mathbf{N}^2$ operator. In deriving the centrifugal distortion terms, the second-order contribution to $\xi_{3/2}(r)$ and $\xi_{1/2}(r)$ is ignored. The matrix elements of H' after the vibrational contact transformation are presented in Table I.

C. Line strength factors and expectation values

In addition to the transition energies calculated from the eigenvalues of the above Hamiltonian, there are several important properties that are calculated from the eigenvectors that aid in understanding the experimental spectrum. These properties include the rotational line strength factors, which are used to understand intensity borrowing in the forbidden transitions, and the expectation value of Λ', which is an index of the amount of mixing between the $B^4\Sigma_u^-$ and $2^2\Pi_u$ states.

TABLE II. Wave numbers of the observed lines in the $B^4\Sigma_u^- - X^4\Sigma_g^-$ system of C_2^+.

N	P_1	P_2	P_3	P_4	R_1	R_2	R_3	R_4
				(0,2) Band of the $B^4\Sigma_u^- - X^4\Sigma_g^-$ system of C_2^+				
1	17 097.6699(6)[a]				17 106.8722(11)	17 107.0861(2)	17 106.7875(8)	
3	17 093.0493(−1)	17 093.2651(5)	17 093.1380(10)	17 092.9128(2)	17 114.5686(17)	17 114.7764(5)	17 114.6798(0)	17 114.4521(−10)
5	17 089.7164(2)	17 089.9258(5)	17 089.8538(1)	17 089.6262(−3)	17 123.5312(12)	17 123.7293(−4)	17 123.6656(−8)	17 123.4338(−1)
7	17 087.6490(8)	17 087.8476(−3)	17 087.7941(−8)	17 087.5629(6)	17 133.7493(5)	17 133.9325(−9)	17 133.8795(−19)	17 133.6341(−16)
9	17 086.8416(−2)	17 087.0256(−8)	17 086.9803(1)	17 086.7332(−13)	17 145.2182(4)	17 145.3741(−21)	17 145.3230(−4)	17 145.0308(−1)
11	17 087.2953(−2)	17 087.4531(−7)	17 087.4026(−21)	17 087.1112(−11)	17 157.9436*[b]	17 158.0368(−17)	17 157.9436*	17 157.7331(6)
13	17 089.0193*	17 089.1121(−12)	17 089.0193*	17 088.8109(10)	17 171.8732*	17 171.8732*	17 172.2351(−17)	17 174.4515(−8)
15	17 091.9564*	17 091.9564*	17 092.3241(−17)	17 094.5402(−12)	17 187.0619(−10)	17 186.2609*	17 186.2609*	17 187.6629(−15)
17	17 096.1786(−14)	17 095.3789*	17 095.3789*	17 096.7834(4)	17 203.4159(5)	17 204.8277(14)	17 205.1370(26)	17 203.9596(−8)
19	17 101.5824(−1)	17 102.9960(25)	17 103.3065(37)	17 102.1298(11)	17 220.6076(38)	17 221.7777*	17 222.1707(18)	17 221.6214(−4)
21	17 107.8448(13)	17 109.0225(−17)	17 109.4102(6)	17 108.8620(−5)	17 241.5309(13)	17 241.3148(−13)	17 240.9741(2)	17 240.5582(−13)
23	17 117.8680(9)	17 117.6524(−12)	17 117.3121(−1)	17 116.8843*	17 261.0153(−20)	17 261.2058(2)	17 261.1148(13)	17 260.7523(−2)
25	17 126.4783(−17)	17 126.6688(5)	17 126.5772(4)	17 126.2159(1)	17 282.3168*	17 282.5758*	17 282.5238*	17 282.1915(−10)
27	17 136.9378(−16)	17 137.1779*	17 137.1779*	17 136.8115(6)	17 304.9512(6)	17 305.1936*	17 305.1936*	17 304.8747(−1)
29	17 148.7548(−12)	17 149.0106*	17 149.0106*	17 148.6820(13)				
				$\Delta J \neq \Delta N$ Transitions				
	$^{P}R_{13}(1)$	17 097.5651(6)	$^{R}Q_{43}(1)$	17 106.6912(0)	$^{R}Q_{21}(1)$	17 106.9579(7)	$^{R}Q_{32}(1)$	17 107.0210(8)
	$^{P}Q_{12}(1)$	17 097.7995(16)						
				(1,3) Band of the $B^4\Sigma_u^- - X^4\Sigma_g^-$ system of C_2^+				
1	17 301.5590(−9)				17 310.6406(−2)	17 310.9076(1)	17 310.5863(12)	
3	17 296.9925(−23)	17 297.2619(−1)	17 297.1038(8)	17 296.8344(5)	17 318.2653(17)	17 318.5287(−13)	17 318.4195(−23)	17 318.1536(−11)
5	17 293.7274(−6)	17 293.9941(−4)	17 293.9096(−2)	17 293.6431(10)	17 327.1592(22)	17 327.4224(−3)	17 327.3545(6)	17 327.0834(−30)
7	17 291.7341(39)	17 291.9965(7)	17 291.9377(8)	17 291.6677(−15)	17 337.3116(28)	17 337.5720(−11)	17 337.5217(−3)	17 337.2554(13)
9	17 290.9967(−2)	17 291.2605(−6)	17 291.2153(−3)	17 290.9478(2)	17 348.7159(15)	17 348.9770(8)	17 348.9358(7)	17 348.6653(−5)
11	17 291.5283(11)	17 291.7911(20)	17 291.7354*	17 291.4812(−9)	17 361.3696(−15)	17 361.6114*	17 361.6114*	17 361.3151(−22)
13	17 293.3213(−1)	17 293.5657*	17 293.5657*	17 293.2704(2)	17 375.2770(12)	17 375.5151*	17 375.5151*	17 375.2375(−12)
15	17 296.3690*	17 296.6162*	17 296.6162*	17 296.3690*	17 390.4260(8)	17 390.6437*	17 390.6437*	17 390.9757(−11)
17	17 300.6990(−3)	17 300.9181*	17 300.9181*	17 301.2517(−6)	17 406.8121(18)	17 406.1419(9)	17 406.3672(9)	17 406.9051(−14)
19	17 306.2760(5)	17 305.6037(−25)	17 305.8323(−2)	17 306.3717(−11)	17 424.3711(−1)	17 424.8089(−3)	17 424.8860(1)	17 424.5294(7)
21	17 313.0486(−18)	17 313.4870(−14)	17 313.5663(3)	17 313.2112(24)	17 443.5622(1)	17 443.8018(−43)	17 443.7182(9)	17 443.4143(17)
23	17 321.4792(−14)	17 321.7253(8)	17 321.6363(−3)	17 321.3350(31)				
				$\Delta J \neq \Delta N$ Transitions				
	$^{P}R_{13}(1)$	17 301.4600(−1)	$^{P}Q_{12}(1)$	17 301.6839(14)	$^{R}Q_{43}(1)$	17 310.4347(−40)	$^{R}Q_{21}(1)$	17 310.7862(13)
				(6,9) Band of the $B^4\Sigma_u^- - X^4\Sigma_g^-$ system of C_2^+				
1					17 184.8022(−19)	17 184.9560(−18)	17 184.7088(6)	
3	17 172.2362*	17 172.4048*	17 172.2362*		17 192.2569(−6)	17 191.9535(17)	17 191.8214(−42)	17 192.3493(−43)
5	17 169.6979(4)	17 169.3861(9)	17 169.2668*	17 169.7823(−8)	17 201.0809(29)	17 201.6106(23)	17 201.6551(12)	17 201.1398(5)
7	17 168.5089*	17 169.0215(21)	17 169.0673(43)	17 168.5089*	17 210.6300(−1)	17 211.2311(6)	17 211.7789(−7)	17 211.3822(−35)
9	17 168.0324(14)	17 168.6266(6)	17 169.1729(9)	17 168.7719(−6)	17 223.3256(−17)	17 223.5396(−9)	17 223.4094(2)	17 223.0391(8)
11	17 170.7198(−10)	17 170.9303(7)	17 170.7948(−4)	17 170.4199(3)	17 236.3237(6)	17 236.5590(17)	17 236.4534(−5)	17 236.0875(−10)
13	17 173.7212(5)	17 173.9506(−11)	17 173.8448(−10)	17 173.4760(−7)	17 250.7638(43)	17 250.9936(−2)	17 250.8984(16)	17 250.5337(21)
15	17 178.1774(23)	17 178.4063(−11)	17 178.3100(10)	17 177.9397(−16)	17 266.5952(1)	17 266.8258(5)	17 266.7290(−15)	17 266.3665(25)
17	17 184.0434(−12)	17 184.2730(−13)	17 184.1779(−15)	17 183.8124(5)	17 283.8133(−22)	17 284.0432(1)	17 283.9510(16)	17 283.5850(33)
19	17 191.3156(−17)	17 191.5444(−16)	17 191.4537(−1)	17 191.0867(0)	17 302.4136(−11)	17 302.6390(−17)	17 302.5460(−26)	17 302.1797(−9)
21	17 199.9888(−5)	17 200.2184(−1)	17 200.1283(−13)	17 199.7647(7)	17 322.3858(−7)	17 322.6137(10)	17 322.5228(−5)	17 322.1573(11)
23	17 210.0604(35)	17 210.2896(13)	17 210.2033(−7)	17 209.8537*	17 343.7310*	17 343.9545(10)	17 343.8672(−10)	17 343.5036(0)

[a]The number in parenthesis denotes observed− calculated line position expressed in terms of the last digits.
[b]The asterisk denotes observed lines that were excluded from the fit as a result of overlapping.

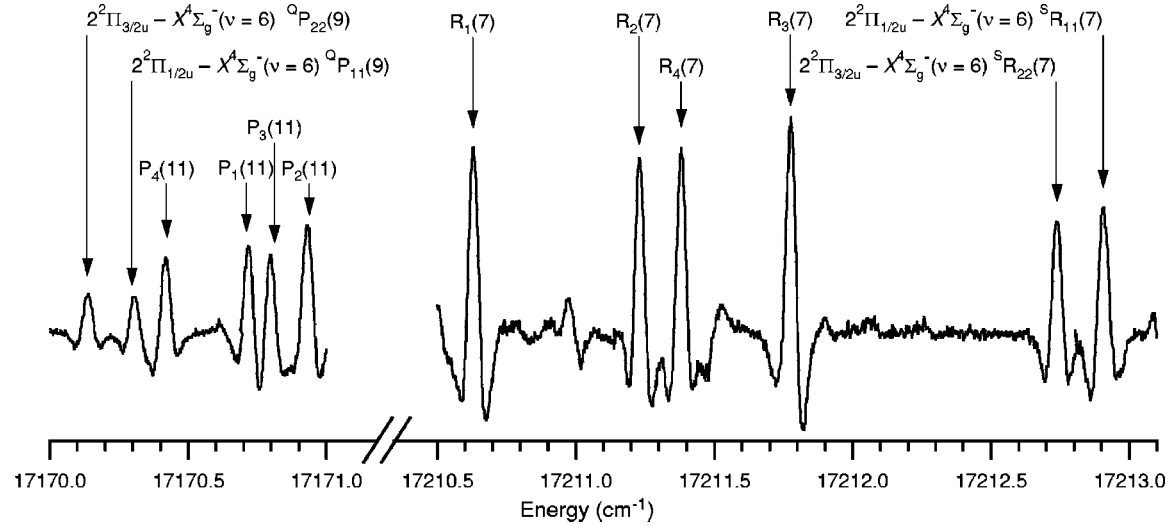

FIG. 3. A portion of the spectrum of the (6,9) band of the $B^4\Sigma_u^- \leftarrow X^4\Sigma_g^-$ transition is shown. The R(7) and P(9) (not shown) quartets are perturbed by both the $\Omega=3/2$ and $\Omega=1/2$ spin–orbit states of the $2^2\Pi_u$ state. In the $B^4\Sigma_u^-$ state, the F_1 component of the $N=8$ level is perturbed by the $J=9.5$ level of the $2^2\Pi_{1/2u}$ spin–orbit state. The mixing of these two states allows for the $^QP_{11}(9)$ and $^SR_{11}(7)$ transitions. Similarly, the F_2 component is mixing with the $J=8.5$ level of the $2^2\Pi_{3/2u}$ state giving rise to the $^QP_{22}(9)$ and $^SR_{22}(7)$ transitions. The P(11) quartet happens to appear near the $^QP_{11}(9)$ and $^QP_{22}(9)$ spectral lines.

The eigenvectors are written as

$$|\Psi''\rangle = \langle X^4\Sigma^-_{g3/2}J''^f_e|\Psi''\rangle|X^4\Sigma^-_{g3/2}J''^f_e\rangle + \langle X^4\Sigma^-_{g1/2}J''^f_e|\Psi''\rangle|X^4\Sigma^-_{g1/2}J''^f_e\rangle, \quad (10)$$

$$|\Psi'\rangle = \langle B^4\Sigma^-_{u3/2}J'^f_e|\Psi'\rangle|B^4\Sigma^-_{u3/2}J'^f_e\rangle + \langle B^4\Sigma^-_{u1/2}J'^f_e|\Psi'\rangle|B^4\Sigma^-_{u1/2}J'^f_e\rangle + \langle 2^2\Pi_{u3/2}J'^f_e|\Psi'\rangle|2^2\Pi_{u3/2}J'^f_e\rangle + \langle 2^2\Pi_{u1/2}J'^f_e|\Psi'\rangle|2^2\Pi_{u1/2}J'^f_e\rangle. \quad (11)$$

The scalar products appearing in Eqs. (10) and (11), e.g., $\langle X^4\Sigma^-_{g3/2}J''^f_e|\Psi''\rangle$, are the numerical elements of the eigenvectors calculated by the fitting routine.

The rotational line strength factors, $S^R_{J'J''}$ are calculated as

$$S^R_{J'J''} = (2J'+1)(2J''+1)\left[\begin{pmatrix} J' & 1 & J'' \\ \frac{3}{2} & 0 & -\frac{3}{2}\end{pmatrix} \times \langle\Psi'|B^4\Sigma^-_{u3/2}J'^f_e\rangle\langle X^4\Sigma^-_{g3/2}J''^f_e|\Psi''\rangle - \begin{pmatrix} J' & 1 & J'' \\ \frac{1}{2} & 0 & -\frac{1}{2}\end{pmatrix}\langle\Psi'|B^4\Sigma^-_{u1/2}J'^f_e\rangle \times \langle X^4\Sigma^-_{g1/2}J''^f_e|\Psi''\rangle\right]^2, \quad (12)$$

where $|\Psi''\rangle$ and $|\Psi'\rangle$ are the ground state and excited state eigenvectors, respectively. Equation (12) is straightforward to derive (see Zare, Sec. 6.5),[27] although the half-integral electronic spin requires careful attention to the phase factors in the derivation. The intensity of a transition is the product of $S^R_{J'J''}$, an oscillator strength factor, a Franck-Condon factor, and a ground-state Boltzmann factor.

The expectation value of Λ' is given by

$$\langle\Lambda'\rangle = |\langle 2^2\Pi_{u3/2}J'^f_e|\Psi'\rangle|^2 + |\langle 2^2\Pi_{u1/2}J'^f_e|\Psi'\rangle|^2. \quad (13)$$

IV. RESULTS AND DISCUSSION

A. The $B^4\Sigma_u^- - X^4\Sigma_g^-$ system

Determination of the line positions of the $2^2\Pi_u \leftarrow X^4\Sigma_g^-$ forbidden transitions required the analysis of the vibronic bands of the $B-X$ system of C_2^+. The analysis is represented as a flowchart in Fig. 2.

The analysis of the Doppler-limited absorption spectrum of the (0,2), (1,3), and (6,9) bands of the $B-X$ system was straightforward. Figure 3 shows a portion of the spectrum. The absorption lines were fit to second-derivative Gaussian line shapes. Overlapped lines were fit simultaneously to a pair of second-derivative Gaussian line shapes. When the resulting rest frequencies of a pair of lines differed by less than 0.02 cm^{-1}, the absorptions were excluded from the data set because the lines were not adequately resolved.

The regions outside the perturbed portion of each band were assigned using the relative intensities from Kovács.[28,29] Then these lines were fit in an initial least-squares fit using the Hamiltonian described in Sec. III and the matrix elements presented in Table I. An iterative approach was used to assign the perturbed portion of the spectrum. The iterative approach consisted of starting outside the perturbed region and gradually working toward the center of the perturbation by adding two to four lines at a time to the initial least-squares fit. Analysis of the (6,9) band was more difficult due to the perturbation occurring at low N. As a result, analysis

TABLE III. Molecular parameters (in cm^{-1}) for the $B^4\Sigma_u^-$, $X^4\Sigma_g^-$, and $2^2\Pi_u$ states of C_2^+.

	(0,2) Band	(1,3) Band	(6,9) Band
$X^4\Sigma_g^-$	$v=2$	$v=3$	$v=9$
B_u	1.380 482(12)[a]	1.362 996(17)	1.253 992(17)
$D_v\times10^6$	6.369(11)	6.448(22)	5.882(23)
$\gamma_v\times10^4$	⋯	⋯	−36.0(19)
$\lambda_v\times10^2$	−6.470(37)	−6.166(42)	−2.612(94)
$\gamma_{Dv}\times10^6$	⋯	⋯	3.955(99)
$B^4\Sigma_u^-$	$v=0$	$v=1$	$v=6$
B_v	1.537 738(12)	1.520 179(17)	1.429 539(17)
$D_v\times10^6$	6.479(12)	6.554(24)	6.834(23)
$\gamma_v\times10^4$	−3.117(89)	−1.10(14)	13.0(18)
$\lambda_v\times10^2$	6.973(40)	7.570(45)	12.167(95)
$2^2\Pi_u$			
B_v	1.181 78(28)	1.108 18(21)	1.0178(15)
$D_v\times10^5$	−3.378(46)	⋯	−21.1(19)
A_v	12.707(65)	9.87(45)	6.720(23)
$A_{Dv}\times10^2$	−0.922(26)	1.59(13)	−4.23(12)
$p_v\times10^2$	−0.155(40)	⋯	−3.830(89)
$q_v\times10^3$	−0.366(34)	⋯	−3.6(11)
Coupling constants			
$\xi_{3/2}$	8.8672(88)	4.0017(58)	3.1670(51)
$\xi_{1/2}$	9.9617(75)	4.550(13)	2.970(10)
$\xi_D\times10^4$	3.78(20)	⋯	⋯
Band origins			
$T_{v'v''}(B^4\Sigma_u^- - X^4\Sigma_g^-)$	17 100.584 44(34)	17 304.331 24(34)	17 178.903 74(56)
$T_{v'v''}(2^2\Pi_u - X^4\Sigma_g^-)$	17 204.350(39)	17 447.014(78)	17 188.767(17)
rms error	0.001 54	0.001 58	0.001 87

[a]The number in the parenthesis denotes one standard deviation expressed in terms of the last digits.

of this band started at higher values of N and iteratively approached lower values of N.

In the preliminary fits of the unperturbed $B-X$ lines, it was necessary to fix γ_v'', γ_{Dv}'', p_v, q_v, $D_{\Pi v}$, and ξ_{Dv} to zero for the (0,2) and (1,3) bands. For the (6,9) band, it was pertinent to include both γ_v'' and γ_{Dv}'' to get a reasonable fit. As more lines of the perturbed region were included in the fits, the excluded parameters mentioned above were added as necessary. In the least-squares fits of the (0,2) and (1,3) bands, γ_v' and γ_v'' cannot be determined independently; because of the selection rules for a $^4\Sigma-{}^4\Sigma$ system, γ_v' and γ_v'' are highly correlated. The consequence in setting $\gamma_v''=0$ is that γ_v' becomes an effective constant approximately equal to $\gamma_v'-\gamma_v''$.

The entire data set for the $B-X$ system includes the following: 94 lines for the (0,2) band with a maximum J of 30.5, of which five lines were transitions where $\Delta J\neq\Delta N$; 77 lines for the (1,3) band with a maximum J of 24.5, of which four lines were transitions where $\Delta J\neq\Delta N$; and 82 lines for the (6,9) band with a maximum J of 24.5. This data set is tabulated in Table II. While spectral lines with higher J values were observed, they were not used in the fit since their F_1 and F_4 components and F_2 and F_3 components were overlapped and difficult to deconvolute.

B. The $2^2\Pi_u-X^4\Sigma_g^-$ forbidden transitions

From the fit of each band, the forbidden transitions and their relative intensities were predicted. In most cases the forbidden transitions were predicted to be within 0.05 cm^{-1} of the actual line position measurement. Each band was refit with its corresponding forbidden transitions; any previously excluded parameters mentioned above were added as necessary. In the least-squares fits: seven forbidden transitions were added to the (0,2) band, four forbidden transitions were added to the (1,3) band, and nine forbidden transitions were added to the (6,9) band. The molecular parameters from the least-squares fits are presented in Table III.

The assignments of the forbidden transitions, their frequencies, and line strength factors, $S_{J'J''}^R$, are presented in Table IV. In addition, Table IV includes the calculated relative intensities for a rotational temperature of 400 K. The intensities presented are relative to the strongest transition in each band, which is the $R_1(9)$ transition in all three bands. The experimentally determined expectation value for the orbital angular momentum $\langle\Lambda'\rangle$ has been included to characterize the amount of Π character in the perturbing state. Unfortunately, many of the frequencies of the forbidden transitions could not be measured as a result of overlapping with other transitions. In this case, their predicted frequencies and uncertainties at one standard deviation are presented in Table IV. Additionally, Table IV presents predicted forbidden transitions, whose intensities were below our detection limit, along with their calculated uncertainties at one standard deviation.

If the interaction was only between the $B^4\Sigma_u^-$ and the $2^2\Pi_u$ states, then the spin–orbit interaction parameters, $\xi_{1/2}$ and $\xi_{3/2}$, would be equal as described in Sec. III B. That is, the ratio, $\xi_{1/2}/\xi_{3/2}$, would be equal to one. A reasonable least-squares fit of the data could not be obtained with the constraint $\xi_{1/2}=\xi_{3/2}$. From the parameters in Table III, the ratio, $\xi_{1/2}/\xi_{3/2}$, for the (0,2), (1,3), and (6,9) bands is 1.1234(14), 1.1370(36), and 0.9378(35), respectively; there-

TABLE IV. The $2^2\Pi_u \leftarrow X^4\Sigma_g^-$ forbidden transitions of C_2^+.

Assign	Wave number/cm^{-1}	Int.	$S^R_{J'J''}$	$\langle \Lambda' \rangle$
	$2^2\Pi_u \leftarrow X^4\Sigma_g^-(v=2)$			
$^{Q}R_{24}(13)$	17 167.7237(19)[a]	0.245	4.42	0.644
$^{O}P_{24}(15)$	17 087.8108(31)*[b]	0.199	4.77	0.644
$^{Q}R_{13}(13)$	17 168.8353(101)*	0.090	1.63	0.877
$^{O}P_{13}(15)$	17 088.9243(101)*	0.073	1.75	0.877
$^{R}R_{12}(15)$	17 198.2497(30)	0.068	1.63	0.901
$^{R}R_{23}(15)$	17 199.0662(28)*	0.067	1.61	0.895
$^{P}P_{12}(17)$	17 107.3648(10)	0.052	1.73	0.901
$^{P}P_{23}(17)$	17 108.1804(−44)	0.052	1.71	0.895
$^{R}R_{23}(17)$	17 189.8328(29)*	0.037	1.22	0.930
$^{R}R_{12}(17)$	17 189.5082(−41)	0.033	1.10	0.940
$^{S}R_{11}(21)$	17 229.4345(295)*	0.029	2.07	0.912
$^{S}R_{11}(19)$	17 234.6391(−5)	0.028	1.36	0.936
$^{P}P_{23}(19)$	17 088.0048(37)	0.027	1.29	0.930
$^{P}P_{12}(19)$	17 087.6794(29)*	0.024	1.16	0.940
$^{Q}P_{11}(21)$	17 121.8793(32)*	0.020	1.42	0.936
	$2^2\Pi_u \leftarrow X^4\Sigma_g^-(v=3)$			
$^{R}R_{12}(17)$	17 409.5644(5)	0.159	5.24	0.715
$^{P}P_{12}(19)$	17 309.0293(1)	0.117	5.53	0.715
$^{R}R_{23}(17)$	17 411.3166(1)	0.081	2.67	0.847
$^{Q}R_{24}(15)$	17 386.5186(1)	0.073	1.73	0.880
$^{P}P_{23}(19)$	17 310.7828(33)*	0.060	2.82	0.847
$^{O}P_{24}(17)$	17 296.7939(33)*	0.056	1.85	0.880
$^{P}R_{14}(13)$	17 371.0942(1651)*	0.007	0.12	0.990
$^{N}P_{14}(15)$	17 292.1993(1650)*	0.005	0.13	0.990
$^{Q}R_{13}(15)$	17 385.3575(864)*	0.005	0.11	0.993
$^{S}R_{11}(19)$	17 440.9091(987)*	0.004	0.18	0.991
$^{S}R_{11}(21)$	17 428.9072(1732)*	0.004	0.25	0.989
$^{O}P_{13}(17)$	17 295.6330(863)*	0.004	0.12	0.993
$^{Q}P_{11}(21)$	17 329.5883(987)*	0.003	0.19	0.991
$^{Q}P_{11}(23)$	17 306.8257(1733)*	0.002	0.27	0.989
$^{S}R_{22}(21)$	17 431.5674(164)*	0.002	0.16	0.993
	$2^2\Pi_u \leftarrow X^4\Sigma_g^-(v=9)$			
$^{S}R_{11}(7)$	17 212.9053(−5)	0.379	3.66	0.611
$^{Q}P_{11}(9)$	17 170.3064(−3)	0.360	4.06	0.611
$^{S}R_{22}(7)$	17 212.7390(−19)	0.353	3.41	0.588
$^{Q}P_{22}(9)$	17 170.1375(11)	0.340	3.83	0.588
$^{P}P_{12}(5)$	17 172.0806(−5)	0.134	1.15	0.776
$^{R}R_{12}(3)$	17 194.6468(−9)	0.115	0.91	0.776
$^{P}P_{23}(5)$	17 172.6149(39)	0.100	0.86	0.793
$^{R}R_{23}(3)$	17 195.1719(−28)	0.079	0.63	0.793
$^{O}P_{24}(3)$	17 173.1290(6)	0.064	0.51	0.580
$^{Q}Q_{23}(1)$	17 185.6695(40)*	0.037	0.28	0.580
$^{P}P_{23}(7)$	17 161.4639(443)*	0.021	0.20	0.968
$^{P}P_{12}(7)$	17 161.5097(382)*	0.020	0.19	0.974
$^{R}R_{23}(5)$	17 194.0548(442)*	0.019	0.17	0.968
$^{R}R_{12}(5)$	17 194.0985(382)*	0.019	0.16	0.974
$^{Q}P_{11}(7)$	17 176.4301(599)*	0.017	0.17	0.980

[a]The number in parenthesis denotes observed−calculated line position expressed in terms of the last digits.

[b]The asterisk denotes predicted transitions with one standard deviation uncertainty expressed in terms of the last digits.

fore the effect of the second-order term in Eq. (5) is experimentally observable.

V. CONCLUSION

The high-resolution absorption spectrum of the (0,2), (1,3), and (6,9) bands of the $B^4\Sigma_u^- \leftarrow X^4\Sigma_g^-$ transition of C_2^+ in the gas phase was obtained using velocity modulation in conjunction with heterodyne detection. The spectrum shows perturbations which are attributed to an interaction between the $B^4\Sigma_u^-$ and the $2^2\Pi_u$ states. The mixing between the $B^4\Sigma_u^-$ state and the $2^2\Pi_u$ state for nearly degenerate levels generated enough intensity borrowing to observe twenty $2^2\Pi_u \leftarrow X^4\Sigma_g^-$ forbidden transitions. The forbidden transitions have been included in a global least-squares fit of each band to obtain improved molecular parameters.

ACKNOWLEDGMENTS

The authors wish to thank Dr. K. Freed for the insightful discussion of C_2^+. We would also like to thank Dr. D. Hullah and Máté Ádámkovics for their earlier work on heterodyne detection. This work was supported by NSF Grant. No. PHY-0099442.

[1] D. Krankowsky, P. Lämmerzahl, I. Herrwerth *et al.*, Nature (London) **321**, 326 (1986).
[2] M. A. Coplan, K. W. Ogilvie, M. F. A'Hearn, P. Bochsler, and J. Geiss, J. Geophys. Res. **92**, 39 (1987).
[3] E. F. van Dishoeck and J. H. Black, Astrophys. J., Suppl. Ser. **62**, 109 (1986).
[4] T. Hasegawa, K. Volk, and S. Kwok, Astrophys. J. **532**, 994 (2000).
[5] T. Oka, J. A. Thorburn, B. J. McCall, S. D. Friedman, L. M. Hobbs, P. Sonnentrucker, D. E. Welty, and D. G. York, Astrophys. J. **582**, 823 (2003).
[6] H. Meinel, Can. J. Phys. **50**, 158 (1972).
[7] C. Petrongolo, P. J. Bruna, S. D. Peyerimhoff, and R. J. Buenker, J. Chem. Phys. **74**, 4594 (1981).
[8] P. Rosmus, H.-J. Werner, E.-A. Reinsch, and M. Larsson, J. Electron Spectrosc. Relat. Phenom. **41**, 289 (1986).
[9] A. O'Keefe, R. Derai, and M. T. Bowers, Chem. Phys. **91**, 161 (1984).
[10] D. Forney, H. Althaus, and J. P. Maier, J. Phys. Chem. **91**, 6458 (1987).
[11] M. Rösslein, M. Wyttenbach, and J. P. Maier, J. Chem. Phys. **87**, 6770 (1988).
[12] J. P. Maier and M. Rösslein, J. Chem. Phys. **88**, 4614 (1988).
[13] F. G. Celii and J. P. Maier, Chem. Phys. Lett. **166**, 517 (1990).
[14] M. Zackrisson and P. Royen, J. Mol. Spectrosc. **161**, 1 (1993).
[15] K. Boudjarane, M. Carré, and M. Larzillière, Chem. Phys. Lett. **243**, 571 (1995).
[16] C. S. Gudeman, M. H. Begemann, J. Pfaff, and R. J. Saykally, Phys. Rev. Lett. **50**, 727 (1983).
[17] C. S. Gudeman and R. J. Saykally, Annu. Rev. Phys. Chem. **35**, 387 (1984).
[18] G. C. Bjorklund, Opt. Lett. **5**, 15 (1980).
[19] R. Wang, Y. Chen, P. Cai, J. Lu, Z. Bi, X. Yang, and L. Ma, Chem. Phys. Lett. **307**, 339 (1999).
[20] S. Gerstenkorn and P. Luc, *Atlas du Spectroscopie d'absorption de la Molecule d'iode* (CNRS, Paris, 1978).
[21] S. Gerstenkorn and P. Luc, Rev. Phys. Appl. **14**, 791 (1979).
[22] J. M. Brown, E. A. Colbourn, J. K. G. Watson, and F. D. Wayne, J. Mol. Spectrosc. **74**, 294 (1979).
[23] K. Kawaguchi and T. Amano, J. Chem. Phys. **88**, 4584 (1988).
[24] J. M. Brown, J. T. Hougen, K. P. Huber *et al.*, J. Mol. Spectrosc. **55**, 500 (1975).
[25] K. F. Freed, J. Chem. Phys. **45**, 4214 (1966).
[26] H. Lefebvre-Brion and R. W. Field, *Perturbations in the Spectra of Diatomic Molecules* (Academic, Orlando, 1986).
[27] R. N. Zare, *Angular Momentum* (Wiley, New York, 1988).
[28] I. Kovács, *Rotational Structure in the Spectra of Diatomic Molecules* (Adam Hilger Ltd., London, 1969).
[29] E. E. Whiting, J. A. Paterson, I. Kovács, and R. W. Nicholls, J. Mol. Spectrosc. **47**, 84 (1973).
[30] Because the interaction between the $2^2\Pi_u$ and $B^4\Sigma_u^-$ states is explicit throughout the electronic contact transformation. All of the sums relating the constants in H_Σ and H_Π to the fundamental molecular Hamiltonian are over all electronic states except for the $2^2\Pi_u$ and $B^4\Sigma_u^-$ states as well. This is the only modification to the relations given by Brown *et al.*